X

Heat generation and losses in carbon nanotubes during field emission

Stephen T. Purcell, Pascal Vincent and Anthony Ayari

X.1 Introduction

Carbon nanotubes (CNTs) have several advantages as field emission (FE) electron sources: chemical stability, high current carrying capacity, high aspect ratios for low extraction voltages and low cost mass production. Since the first experiments [1,2,3] many authors have shown the extraction of both stable and very large FE currents, I [4,5,6,7,8]. This opens numerous commercial applications which often demand the highest possible currents. It is now clear that this is controlled by the interplay between Joule heating effects either along the nanotube lengths [9,10] or at the contact [11,12], and stabilising heat evacuation mechanisms.

The particularity of CNT field emitters is that they emit stably in a high temperatures state induced by the Joule heating, eg. up to ~1600 K. The stable heating state is not often observed for emitters of other materials and has far ranging implications. It increases sustainable high currents, permits self-cleaning by desorption that improves dramatically the current stability, causes CNT shortening instead of sudden breakdown at extreme currents and finally it allows measurements of several intrinsic parameters of the carbon nanotube [13]. In contrast, metal tip emitters suddenly melt into large balls near the apex at high current densities due to catastrophic runaway phenomenon that quickly follows induced heating [14,15]. Three positive feedback mechanisms accentuate temperature and current increases and thus breakdown: (1) the strong increase in the metallic resistance with temperature, (2) the increase in FE with temperature and (3) the rapid diffusion of metal surface atoms to high field regions, particularly as temperature increases, which sharpens tips and thus further increases current. Here we review the current state of experimental studies and theoretical understanding of the generation and evacuation of heat in carbon nanotubes during FE. Experimental measurements of the temperature by Field Electron Emission Spectroscopy (FEES) measurements of Total Energy Distributions (TEDs) [16,17] are emphasised, but other

pertinent results are surveyed. The basic theoretical framework is given for heat generation and evacuation accompanied by simulations. An effort is made to show how this is a very open and eventually complex subject with as yet far from quantitative agreement between experiment and theory.

Heating effects were reported in one of the very first articles on FE from CNTs [1], though the heating was induced by a focused laser. Light emission ascribed to black body radiation was also observed. We limit our discussion here to current-induced heating. The stability of the FE current from carbon nanotubes was studied early on and discussed within the framework of adsorption and ion retro bombardment [18,19]. Observations of a gradual destruction of arc electric MWNTs at currents as high as 200 μA during FE were made inside a transmission electron microscope (TEM) [20], though the probable cause by Joule heating was not yet evoked. Heating was originally hypothesised to explain high current behaviour and degradation of CNTs [21] due to local heating near the apex by Nottingham effects [16] through resonant tunnelling states. As well the existence of characteristic rings in the FE patterns, observed previously [19], was used to estimate that field-assisted evaporation of single wall nanotubes (SWNTs) starts at ~1600 °C. The origin of the rings was unclear at that time but we have recently shown that they can be explained by self-focusing of thermal-field electrons from the shank just below the cap of a hot nanotube [22], thus confirming the determination of the temperature in [21].

The role of Joule heating was clearly established by FEES on an individual MWNT [9]. This was used to: (1) measure the temperature at the emission zone as a function of emission current, $T_L(I)$ (L=CNT length); (2) show that I~μA induced high stable temperatures reaching 2000 K; (3) measure the electrical resistance of an individual MWNT, R(I) (equivalently $R(T_L)$), in this case ~MΩ; (4) show that the high temperatures were accompanied by light emission from the MWNTs whose intensity was consistent with Planck's law; (5) show that the high induced temperatures can lead to excellent emission stability by self-cleaning the surfaces of the nanotubes; (6) show that even higher currents, and thus higher temperatures, leads to a gradual destruction of the nanotubes. These studies were accompanied by confirming simulations of a 1D model [10] that incorporated Joule heating, thermal conduction to the support, radiation losses and Nottingham effects. Nottingham effects were estimated to be small compared to Joule heating, thermal conduction and radiation. This work also showed that FE becomes a new tool for making simultaneous, and therefore correlated, measurements of several CNT physical properties.

Since this work, optical spectroscopy measurements of light emission from a MWNT layer from which a small number of emitters were active confirmed that the light has a black body spectrum [23]. Experiments and extension of the modelling of [10] on emission from vertical CNTs on Si substrates were used to compare and predict the critical field, current density and currents for thermal runaway in CNTs when the electrical resistivity, $\rho(T)$, increases at higher temperature consistent with phonon controlled mean free paths [12]. 1D modelling was carried out that particularly addressed the Nottingham effect [24] predicting that in certain conditions they can be stronger than radiation effects. A fuller account of the data of [9] and somewhat refined

modelling of [10] was presented [25] with a better function for $\rho(T)$, and for the first time an estimate of the temperature dependence of the thermal conductivity $\kappa(T)$. Another aspect was the integration of the TEDs to quantify the Nottingham energy exchange at different temperatures and emission zones. More recently the 1D model was used to study the influence of Nottingham effects particularly at high currents and temperatures [26]. In this region it may cause cooling and the temperature at the CNT cap can be lower than the near cap region. Finally, 3D simulations have been made [27] that compare Joule and Nottingham heating without radiation and allow for temperature increases in a W support tip. It was concluded that Joule heating is orders of magnitude larger for currents above pA. Thus different authors have come to different conclusions for the influence of Nottingham effects and more work is needed. This may be because the various mechanisms have different scaling (see below) and each author simulated the problem with different parameters, or because more complex averaging of Nottingham effects over the emission surface is necessary for it to be well quantified [25].

X.2 Heat diffusion equation for nanotubes

The measurement and calculation of temperature profiles in nanotubes (and nanowires) is actually a very challenging and open problem that can be treated at many levels of complexity. Our approach has been to find the simplest approximations that contain the essential physics. The nanotube is treated as a simple resistance which is justified for many nanotubes, e.g. MWNTs produced by chemical vapor deposition (CVD), because mesoscopic behavior such as ballistic transport of electrons and phonons observable in high quality CNTs produced by arc discharge is quickly masked by defects and phonon scattering, particularly at room temperature and above. The simplest model is to treat the CNT as a one dimensional object of length L in contact with a heat sink fixed at temperature $T=T_0$ at x=0 and include heat generation and losses by (1) Joule effects, (2) thermal conduction, (3) radiation and (4) Nottingham exchanges at the CNT cap.

The first two mechanisms should be well enough described by classical expressions. However we and others [10,12,24,26] have modelled the radiation losses by a differential surface area and the Stefan Boltzmann law with a constant emissivity. This is clearly not correct [25] because the diameter of most nanotubes is less than the wavelength and mean free path of photons and thus a differential element must radiate by its volume and not its surface. Photon emission should be considered within the framework of Rayleigh scattering, where absorptivity, a, and hence emissivity, e, depend on the particle dimensions, thus adding considerable complexity to the problem. For example, for a small enough dielectric sphere $a(r, \lambda) = (r/\lambda)f(n)$ where f(n) is a dimensionless function of the complex index of refraction, n [28]. Evoking Kirchoff's law and inserting this into the Stefan-Boltzman law makes emitted power proportional to volume as expected. Unfortunately this is not sufficient here because antenna and polarized light emission effects must be treated and most nanotubes are not dielectrics. It is not even evident that a local differential expression for radiation losses is appropriate. Doing this correctly may completely change the balance between radiation, thermal conduction and Nottingham effects. Nottingham effects can be included as a boundary condition for heat flow at the cap, $J_{Th}(L)$ [10,24,25,26,27]. Until now the maximal

current density and field at the cap apex have been used to calculate exchanges but this is a rough approximation that favors heating [25]. The expression should be integrated over the cap apex where lower fields favor cooling as opposed to heating. In the absence of better expressions we proceed as before with the idea that including the dominating T^4 factor and Nottingham effects at the apex allow discerning general trends.

Under the simplest assumptions, the time-independent heat diffusion equation will be:

$$\rho(T)I_{FE}^2\frac{dx}{A}+\kappa(T)A\frac{d^2T}{dx^2}dx-2\pi\, re(r)\sigma(T^4-T_0{}^4)dx=0 \qquad \text{X.1}$$

$\rho(T)$ and $\kappa(T)$ are the temperature dependent resistivity and thermal conductivity, A is the cross-section, r the exterior tube radius, σ the Stefan-Boltzmann constant and T_0 the ambient temperature at the support/CNT contact. For all simulations below we assume $e(r)=1$ and $A=\pi r^2$ which is a good approximation for nanotubes with the more common central tube diameters. The Nottingham boundary condition at the cap is

$$J_{Th}(L)=I_{FE}\langle E\rangle=-\kappa(T)A\frac{dT}{dx} \qquad \text{X.2}$$

where <E> (in eV) is the average energy of emitted electrons with respect to the Fermi level (<E><0, heating, <E>>0, cooling). <E> can be estimated with the TEDs.

A useful analytic solution can be given when radiation is neglected and κ and ρ are constant which is reasonable for low temperatures:

$$T(x)=T_0+\left(\frac{\rho}{\kappa}\frac{I^2}{A^2}-\frac{I\langle E\rangle}{\kappa A}\right)x-\frac{\rho}{2\kappa}\frac{I^2}{A^2}x^2 \qquad \text{X.3}$$

$$\text{At } x=L,\ T_L=T_0+\frac{\rho}{2\kappa}\frac{I^2}{A^2}L^2-\frac{I\langle E\rangle}{\kappa A}L \qquad \text{X.4}$$

The Nottingham/Joule ratio scales with $\eta_{NJ}\equiv 2\langle E\rangle A/\rho IL$. This varies widely for nanotubes, perhaps explaining why different results have been reported.

To get a feeling for heating effects consider a reasonable parameter set (in SI): $\rho=10^{-5}$, $\kappa=100$, $L=10^{-6}$, $I=10^{-5}$, $A=10^{-16}$ and $\langle E\rangle=-0.1$(heating). One gets $\Delta T\equiv T_L-T_0=500+100=600°$. However, the formula gives wildly varying estimates for physically possible nanotubes. A particularity of carbon is that $\rho(T)$ and $\kappa(T)$ both vary by orders of magnitude for different forms of graphite [29] and for nanotubes, and they are particularly sensitive to different heat treatments. Obviously the dimensions of nanotubes also vary by orders of magnitude. Though we assume here ideal structures, in reality the overall radius, the ratio of the inner/outer tube radii and the structural quality are often not uniform. $\rho(T)$ and $\kappa(T)$ may also vary with position along the tube because the CNTs may undergo temperature gradients. Finally, as stated above, η_{NJ} can vary greatly. This means that each nanotube must be specifically analyzed and one needs the maximum information to understand high current and temperature behavior.

X.3 Simulations

Solving equation X.1 numerically by iteration is simple if all the CNT parameters are known. Typical examples with and without radiation included are shown Figure X.1(a,b) for T(x) and $T_L(I)$. Nottingham effects are neglected. One sees that the difference in temperatures for calculations that include either a decreasing ρ(T) or radiation losses, progressively increases with temperature. The analytical form is accurate for $\Delta T<500$ for this choice of parameters.

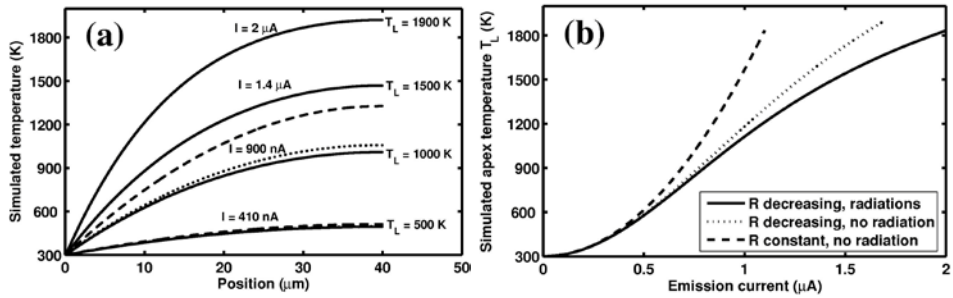

Figure X.1 (a)(b) Temperature profiles along a CNT and $T_L(I)$ for different cases simulated using Eqs. X.1, or X.3 and X.4 (L=40 μm, r=10 nm). Dashed curves: κ=100 and $\rho=1.6\times10^{-5}$, no radiation (Eqs. X3, X4). Dotted curves: $\rho(T)=1.6\times10^{-5}-6.4\times10^{-9}$(T-300), no radiation. Solid curves: same with radiation losses included (see [10]).

Though r, A and L can be determined by electron microscopy, generally one does not know *a priori* ρ(T), κ(T), e(r,T) and <E>. Thus one of the goals of this work is to use FEES experiments and simulations to extract these functions from the data.

In experiments one generally imposes an applied voltage, V, and measures the emitted I which adds an additional degree of complexity to the problem. Using the measured I is sufficient for resolving equation X.1, but does not address questions such as the existence of a solution for an elevated stable temperature and the high current degradation where current changes in time. Actually I increases with T_L and this creates positive feedback. A self-consistent solution between the FN equation and the heat equation is needed to find the equilibrium points of V, I, and T_L (and T(x)). For this it is convenient to use a graphic representation where $T_L(I)$ and the thermal $I(V,T_L)$ evolution are plotted on the same graph. We use Eq. X.1 with R and κ constant to obtain $T_L(I)$ without loss of generality. Consider a CNT (SI units) with $L=10^{-5}$, $r=1.5\times10^{-9}$, $\rho=2.6\times10^{-5}$, κ=100, and T_0=300 K. Furthermore, consider a constant field enhancement factor β (field=βV), no effect of an IR drop along the CNT and the thermal dependence of the FE current given by $I(V,T_L)\cong I(V,T_L=0)\times(1+\text{const}.T_L^2)$ [16]. For a given voltage, V_1, $I(V_1,T_L=0\text{ K})$ defines a point on the x-axis (see Figure X.2(a)). The emission would start slightly above at $I(V_1,300K)$ if the voltage is applied much faster than heating occurs. $I(V_1,T_L)$, is given by the parabolic red curve (the inverse function $T_L(V_1,I)$) starting from this point. The self-consistent solution of the thermal and FE equations is the intersection of the red curve and the black curve to give the set V_1, T_{L1} and I_1. In time I would move along the $I(V_1,T)$ curve. For increasing voltages we obtain other red

curves and new stability solutions. Depending on the $T_L(I)$ curves there is a maximum voltage above which no stability point exists (voltage V_2 in the figure). This defines the maximum temperature, T_M, and current for which the system is stable. This analysis explains in a simple way the critical temperature, current and field calculated previously [12] versus the CNT length. At higher voltage, i.e. V_3, there is no stationary solution and I and T_L should increase without bounds. T_L and I must then be calculated by the non stationary diffusion equation. Note that the CNT may degrade at a temperature inferior to the maximum mathematical stability point because carbon leaves the CNT cap.

From Fig X.2(b) one sees that two solutions are expected, T_1 and T_2, for a voltage slightly lower than V_2, one inferior and one superior to T_M. These two solutions exist mathematically but T_1 is structurally stable and is the only physical solution. T_2 is structurally unstable and cannot be a physical solution. However this unstable point could be found by numerical calculations and must be recognized as such.

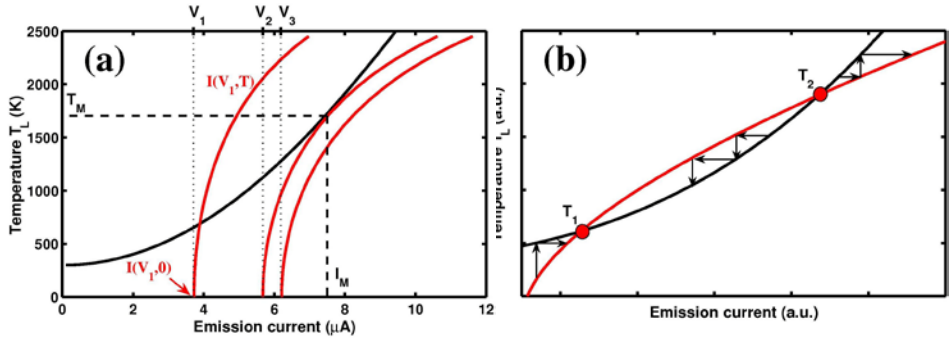

Figure X.2(a). Plots of $T_L(I)$ from simulations using Eq. X.1 and $I(V,T_L)$ (inverted axis). The crossing points define the equilibrium parameter set (V,I,T_L). (b) Zoom near an equilibrium point showing that there are two solutions. The upper solution is unstable (see text) and simulations will follow the arrows.

This is the analysis of the simplest situation but many different cases can be envisaged. For example, a decrease in $\rho(T)$, increase in $\kappa(T)$ and Nottingham effects may cause the $T_L(I)$ curves to bend downward further thus pushing the intersection points to higher currents. Also a $\rho(T)$ that increases with T at higher temperatures [12] could cause $T_L(I)$ to increase again at higher currents, perhaps creating more equilibrium points and thus hysteresis effects. For certain parameter sets, $T_L(I)$ and $I(V,T_L)$ may run roughly parallel, leading to slow responses of the system. In fact we once observed the current from a nanotube at fixed voltage slowly increasing by over 100% during roughly a ten second time frame, while its incandescence also increased greatly, until it suddenly broke down at 40 μA. This is a very long time for a heating phenomenon in a nanometric object.

The cap region has the highest temperature and field during current-induced heating and thus CNT degradation occurs there preferentially. Regular thermal removal of material at the nano or atomic scale should roughly follow an Arrhenius relation, with an average activation energy. Thus time scales are controllable if temperature is controlled. Through current-induced heating it is possible to observe and control CNT length reduction on a

lab time scale in both simulations and experiments. The gradual degradation phenomenon was first studied in a TEM [20] and then by following I and FEM patterns in time [21] (see also [25,30]. Notably in [21] the carbon atoms could leave the SWNTs ring by ring. Striking results from recent detailed TEM studies [31,32] are shown in Figure X.3(a)(b) which demonstrate the gradual and controlled shortening of a MWNT and accompanying I(V) characteristics. The series of I(V) characteristics have a well defined envelope. This effect has recently used to precisely tune the resonance frequencies of CNTs in a TEM [33]. Simulations must now include self-consistent solutions between the FN equation and the heat equation in which the length of the CNT also changes. This can be carried out to different degrees of sophistication. Here we simply limit the length by imposing a maximum temperature at the CNT cap. Changes on a lab time scale (tens of seconds) is known to occur in the 1600 to 2000K [9,21] range. The envelope of calculated curves in Figure X.3(b) are similar to the experimental

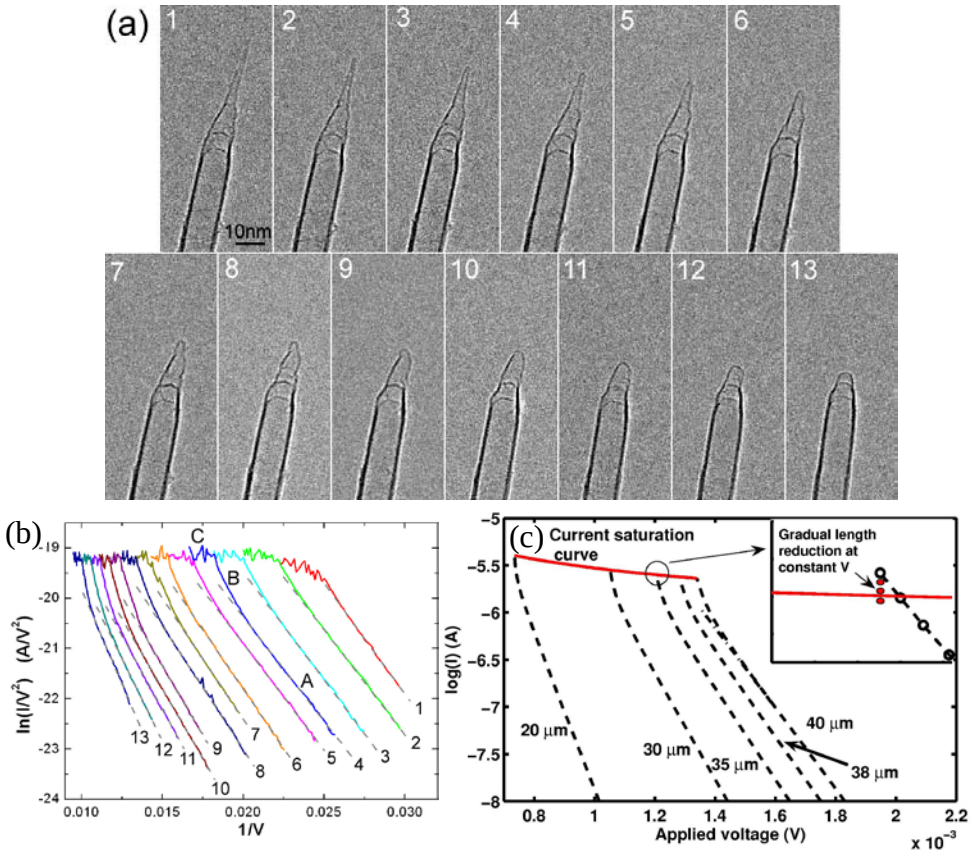

curves of Fig. X.3(b) and [30], showing that the regular and reproducible material loss at the apex region can be well simulated and thus understood.

Figure X.3(a) TEM images showing the controlled shortening of conical CNT tips by current induced heating. (b) Corresponding F-N plots ((a),(b) [32] with permission). (c) Simulated I(V) curves for the shortening of CNT at a set temperature [30]..

X.4 Experiments

Our group has studied high current behaviour particularly with FEES to characterize individual MWNT at various stages of the thermal and field cleaning of MWNTs. The results were then analyzed by running specific simulations with the heat diffusion equation X.1. The FEES permits simultaneous measurements of both $T_L(I)$ and the voltage drop without which it is difficult to imagine providing meaningful comparisons between theory and experiment, particularly without *a priori* knowledge of $\rho(T)$,$\square\kappa(T)$, e(r,T) and <E>. Unfortunately there is only one published set of data [9,25] that measures simultaneously $T_L(I)$ and $R(T_L)$ to guide calculations. The result is that in our opinion though the first order description of the problem is now in place, quantitative comparisons with theory and experiment are largely lacking. This effectively excludes examining many interesting second order effects.

The details of the experimental procedure are described in the original articles. The experiments were carried out in an ultra high vacuum (UHV) system fully equipped for measuring field electron microscopy (FEM) and field ion microscopy (FIM) and FEES. Oriented MWNTs were grown by chemical vapour deposition (CVD) directly on large Ni support tips. Scanning electron microscopy (SEM) showed that the apex MWNTs were quite straight, with diameters in the range of 20 to 50 nm and had lengths up to ~ 40 μm. The multiwall character, diameter range and high number of defects of the MWNTs were confirmed by TEM on samples fabricated by exactly the same procedure. The Ni tip was held in a W spiral to allow in-situ cleaning by standard Joule heating to ~ 1300 and up to 1600 K by electron bombardment. The TEDs were measured with a hemispherical electron energy analyzer through a probe hole in the same UHV system. Though many MWNTs are present on the Ni tip, the FE experiments are specific to an individual one because of the selectivity of FE to the highest field emitters.

Two distinct emission regimes before and after the highest temperature cleaning were observed. The first regime is when the surface is rough and consists of disordered nanostructures formed either by adsorbates or the carbon itself. These objects give rise to strong effects in the TEDs similar to those measured from deposited molecules [34]. The resonant tunnelling model [35] has been often invoked to explain most of the effects [25]. The second regime, the "intrinsic MWNT emitter", is when the surface was heated to temperatures reaching 1600 K to produce a "smoother-cleaner" surface without nanometric protrusions. I/V characteristics and TEDs then followed FN theory and excellent current stability was achieved.

The formula for the TED of FE from a free electron gas [16] is the product of a field-dependent transmission probability and the Fermi-Dirac distribution:

$$J(E)\ \alpha \frac{\exp((E-E_F)/d)}{1+\exp((E-E_F)/k_B T_L)} \quad . \qquad \text{X.5}$$

E_F is the Fermi energy and $d(eV) \sim F/\sqrt{(\phi)} \sim 0.2$ eV. F is the applied field (~3-7 V/nm) and ϕ the work function in eV. The TEDs are asymmetric peaks of width ~0.3 eV at room temperature. The slope of ln(J(E)) on the low energy side is 1/d and on the high energy side $(1/d\text{-}1/k_BT) \sim -1/k_BT$. The peak is positioned close to E_F. In general the experimental measurements of TEDs from metallic emitters deviate somewhat from this formula [16]. However the key to these experiments is that they permit an excellent measure of E_F and the temperature at the emission zone. We have found agreement within 20 K between optical pyrometry measurements and fits to X.5 in the 1000 to 1300 K range when the temperature was controlled by the support heating loop, and better than 0.05 eV for E_F for emission from W and Pt emitters in the same setup. Three series of TEDs were measured through the probe hole. TEDs from the brightest FE zone (series 1) at various I_{FE} are shown in Figure 4(a). As the voltage and I were increased the TEDs widened on the low energy side as expected and also shifted to lower energy, due to a resistance drop along the MWNT, and widened on the high energy side, due to significant heating effects. We have fitted the data to X.5 to extract the dependence of the parameters E_F, T_L and d on the voltage and current.

In Figure 4(b) we show the fits to the measured TEDs with equation X.5 for E_F against applied voltage and current. They show that E_F displaces to lower energy roughly linear with I because of a resistive IR drop along the MWNT. The shift gives resistances in the MOhm range. In Figure 4(c) we show that T_L increased from 300 K ($I < 1$ nA) to 2000 K ($I = 2.3$ μA). The results for two runs on different emission zones are shown. As a direct consequence of these results we proposed that heating rises occur because of Joule heating along the MWNT. The simultaneous direct measurement of temperature and resistance give the necessary inputs for simulation of the heat diffusion problem [10].

The combination of independent measures of temperature and resistance allow us to determine the nanotube resistance $R(T_L) \equiv E_F/I_{FE}$ which was in the MΩ range. It decreased as T_L increased by ~70 %. (see Figure 4(d)) showing that this MWNT did not have metallic behaviour. This $R(T_L)$ was used by all those who have made simulations of the FE current induced eating problem in CNTs [10,12,24,26,27]. Also shown is the fit to this data using the heat equation allowing for a variable electrical and thermal conductivity. $R(T_L)$ (and hence $\rho(T)$) is an exponentially decreasing function and $\kappa(T)$ increases linearly with T (see Figure X.4(d)). The average values are both in the range of disordered graphite [29] which can be understood from the TEM images showing many defects. The length and diameter of the MWNT are rather approximate so the absolute values are crude. However the ratio $\rho(T)/\kappa(T)$ and the general temperature dependence do not vary strongly with the nanotube dimensions and thus these simulations provide a proof-of-concept for the technique.

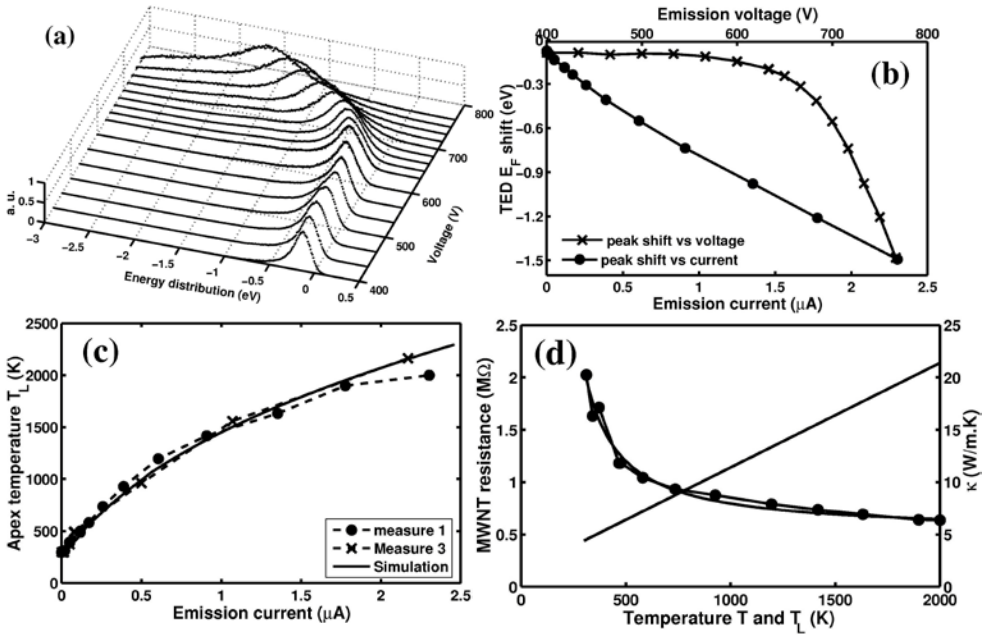

Figure X.4(a) Series of TEDs for the MWNT after electron bombardment heating to 1600 K. (b) Shifting of the TEDs with current and voltage showing that the displacement is due to an IR drop. (c) Temperature at the MWNT cap, T_L, measured by fitting the TEDs for two runs. The solid line is a fit to the $T_L(I)$ curve using simulations of the heat equation that determines $\rho(T)$ and $\kappa(T)$. (d) $R(T_L) \equiv E_F/I$ from fitting the TEDs. $\kappa(T)$ is found through self-consistent simulations with equation X.1 (A=314 nm^2 and L=40μm).

One of the consequences of the heating is that the current rises above the FN line at high currents and temperatures above ~1000K [21,9,24] as shown in Figure 5(a). This is the direct consequence of the increase of $I \alpha T^2$ in FN theory [16] which we used above. In Inset in Figure 5(a) we plot the difference between the FN fit at low voltage and the measured data against the measured T_L. The fit to the T^2 law is rather good except for the last two points which mark the temperature at which the MWNT undergoes length reduction by partial destruction.

A final consequence of the heating that we treat here is an increase in FE current stability. In Figure X.5(b) we show that the current induced heating can be used to thermally remove adsorbates allowed to accumulate by exposure to a poor vacuum. This was demonstrated by stopping the pumping to allow the vacuum to degrade to the 10^{-7} Torr range, leading to an extremely unstable current (Figure X.5(b)). After a 10 sec flash of 1 μA FE emission, which according to the TEDs raised the temperature to ~1000 K, I became as stable as before. I is even more stable at higher current because the hot nanotube prevents re-adsorption as is well known for Schottky emitters. Figure 5(b) shows an almost perfect stability obtained at 1 μA during three hours. The treatment at 1

μA thus has an effect comparable with a flash surface cleaning, but without any external heat source.

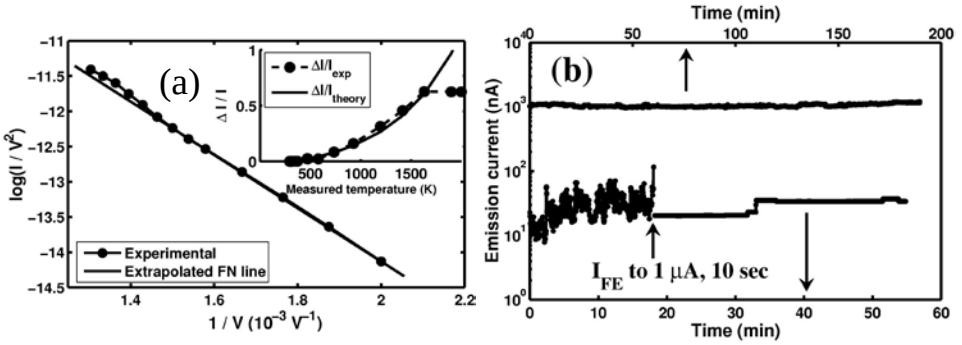

Figure X.5(a). FN plot corresponding to Figure X.4(a). The current rises above the FN line because of the current-induced high temperature. Inset: Difference between the measured current and the low current fit to the FN plot as a function of T_L. (b) Current stability measured before and after a current induced heat flash of 10 s and a 3 h current stability run at 1 μA.

CONCLUSION

In this article we have tried to bring out the advances in our understanding of temperature effects in field emission from nanotubes and point out where more work is needed. For the cleaned emitters, what distinguishes CNTs is their ability to function over long times in a condition of current-induced high temperature. This is because of the intrinsic decrease in the MWNT resistance with temperature and the low surface diffusion of carbon prevents them from falling immediately into a current runaway and explosive breakdown common to metal emitters. The nanotube resistive heating is a tool to preferentially clean the principle emitters in an ensemble without external heating. This may be the reason that such excellent stability has been achieved in CNT flat screens where the vacuum conditions are far from UHV. The gradual length reduction at higher currents provides a tool for more uniform emission from a multi-nanotube emitter at the price of higher extraction voltage. This is useful in applications such as displays where uniformity is critical.

Modelisation of the heat transport problem is essential for exploiting the FEES data to extract simultaneous estimates of the physical parameters of CNTs. It permitted estimate s of $\rho(T)$ and $\kappa(T)$ together for the first time. Measurements on different types of CNTs with a better characterization of their crystalline structure and dimensions are now needed for more quantitative calculations. The theory can then be extended to better include advanced models of the Nottingham effects and radiation cooling.

In conclusion, the combination of $\rho(T)$ and $\kappa(T)$ estimates, the optical emissions and the in situ excitation of mechanical resonances [36] now gives FE access to four fundamental characteristics of a single nanotube or nanowire.

[1] Rinzler, A.G. Hahner, J.H. Nikolaev, P. Lou, L. Kim, S.G. Tomanek, D. Nordlander, P. Colbert and D.T. Smalley, R.E., 'Unraveling nanotubes: field emission from an atomic wire', *Science*, **269**, 1995, 1550-1553.
[2] de Heer, W. Châtelain, A. Ugarte, D., 'A Carbon Nanotube Field Emission Electron Source', *Science*, **270**, 1995, 1179-1180.
[3] Chernozatonskii, L.A. Gulyaev, Yu.V. Kosakovskaja, Z.Ja. Sinitsyn, N.I. Torgashov, G.V. Zakharchenko, Yu.F. Fedorov and E.A. Val'chuk, V.P., 'Electron field emission from nanofilament carbon films', *Chem. Phys. Lett.*, **233**, 1995, 63-68.
[4] Fransen, M.J. van Rooy and T.L. Kruit, P., 'Field emission energy distributions from individual multiwalled carbon nanotubes', *Appl. Surf. Sci.*, **146**, 1999, 312-327**.**
[5] Lovall, D. Buss, M. Graugnard, E. Andres R.P. and Reifenberger, R., 'Electron emission and structural characterization of a rope of single-walled carbon nanotubes', *Phys. Rev. B*, **61**, 2000, 5683-5691.
[6] Bonard, J.-M. Kind, H. Stöckli, T. and Nilsson, Lars-Ola, 'Field emission from carbon nanotubes: the first five years', *Solid State Electronics*, **45**, 2001, 893-914.
[7] de Jonge, N. and Bonard J.-M., 'Carbon nanotube electron sources and applications', Phil. Trans. Roy. Soc. Lond. A, 362, 2004, 2239-2266.
[8] Minoux, E. Groening, O. Teo, K.B.K. Dalal, S.H. Gangloff, L. Schnell, J.-P. Hudanski, L. Bu, I.Y.Y. Vincent, P. Legagneux, P. Amaratunga G.A.J. and Milne, W.I., 'Achieving high-current carbon nanotube emitters', *Nanoletters*, **5**, 2005, 2135-2138.
[9] Purcell, S.T. Vincent, P. Journet, C. and Binh V.T., 'Hot nanotubes: stable heating of individual multiwall carbon nanotubes to 2000 K induced by the field-emission current', *Phys. Rev. Lett*., **88**, 2002, 105502.
[10] Vincent, P. Purcell, S.T. Journet, C. and Binh V.T., 'Modelization of resistive heating of carbon nanotubes during field emission', *Phys. Rev. B*, **66**, 2002, 075406.
[11] J.-M. Bonard, C. Klinke, K.A. Dean and B.F. Coll, 'Degradation and failure of carbon nanotube field emitters', *Phys. Rev. B*, **67**, 2003, 115406.
[12] Huang, N.Y. She, J.C. Chen, Jun Deng, S.Z. Xu, N.S. Bishop, H. Huq, S.E. Wang, L. Zhong, D.Y. Wang and E.G. Chen D.M., 'Mechanism Responsible for Initiating Carbon Nanotube Vacuum Breakdown', *Phys. Rev. Lett.*, **93**, 2004, 075501.
[13] Purcell, S.T. Vincent, P. and Journet, C., 'Measuring the physical properties of nanostructures and nanowires by field emission', *Europhysics News*, **37**(4), 2006, 26-28.
[14] Dyke, W.P. Trolan, J.K. Martin, E.E. and Barbour, J.P., 'The Field Emission Initiated Vacuum Arc. I. Experiments on Arc Initiation', *Phys. Rev*., **91**, 1953, 1043-1054.
[15] Dolan, W.W. Dyke, W.P. and Trolan, J.K., 'The Field Emission Initiated Vacuum Arc. II. The Resistively Heated Emitter', *Phys. Rev.*, **91**, 1953, 1054-1057.
[16] See for example, Swanson, L.W. and Bell, A.E. in '*Advances in Electronics, Electron Physics'*, **32** (Ed. Marton, L.), Academic Press, New York, 1973.
[17] see for example J.W. Gadzuk, E.W. Plummer, 'Field Emission Energy Distribution (FEED)', *Rev. Modern Phys*., **45**, 1973**,** 487-548.
[18] Bonard, J.-M. Salvetat, J.P. Stöckli, T. Forro, L. and Chatelain, A., 'Field Emission from carbon nanotubes: perspectives for applications and clues to the emission mechanism', *Appl. Phys. A*, **69**, 1999, 1-10.
[19] Dean, K.A. von Allmen, P. and Chalamala, B.R., 'Three behavioral states observed in field emission from single-walled carbon nanotubes', J. Vac. Sci. Technol. B **17**, 1999, 1959-1969.
[20] Wang, Z.L. Poncharal P. and de Heer, W.A., 'Nanomeasurements in transmission electron microscopy', *Microsc. Microanal*., **6**, 2000, 224-230.
[21] Dean, K.A. Burgin, T.P. and Chalamala, B.R., 'Evaporation of carbon nanotubes during electron field emission', *Appl. Phys. Lett*., **79**, 2001, 1873-1875.
[22] Marchand, M. Journet, C. Adessi C. and Purcell, S.T., in preparation.
[23] Sveningsson, M. Jonsson, M. Nerushev, O.A. Rohmund, F. Campbell and E.E.B., 'Blackbody radiation from resistively heated multiwalled carbon nanotubes during field emission', *Appl. Phys. Lett.*, **81**, 2002, 1095-1097.
[24] Sveningsson, M. Hansen, K. Svensson, K. Olsson, E. Jonsson, M. Campbell, E.E.B., 'Quantifying temperature-enhanced electron field emission from individual carbon nanotubes', *Phys. Rev. B.*, **72**, 2005, 085429.
[25] Purcell, S.T. Vincent, P. Rodriguez, M. Journet, C. Vignoli, S. Guillot, D. and Ayari A., 'Evolution of the Field-Emission Properties of Individual Multiwalled Carbon Nanotubes Submitted to Temperature and Field Treatments', *Chem. Vap. Deposition*, **12**, 2006, 331–344.

[26] Wei, W. Liu, Y. Wei, Y. Jiang, K.L Peng, L.-M. and Fan, S.S., *Nanoletters*, 'Tip cooling effect and failure mechanism of field-emitting carbon nanotubes', **7**(1) 2007, 64-68.
[27] Sanchez, J.A. Mengüç, M.P. and Hii, K.-F., 'Heat Transfer Within Carbon Nanotubes During Electron Field Emission', *Journal of Thermophysics and Heat Transfer* **22**, 2008, 281-289, and Sanchez, J.A. Mengüç, M.P, 'Geometry dependence of the electrostatic and thermal response of a carbon nanotube during field emission', *Nanotechnology*, **19**, 2008, 075702.
[28] Craig F. Bohren and Donald R. Huffman, *'Absorption and Scattering of Light by Small Particles'*, John Wiley and Sons, New York, 1983.
[29] Kelly, B.T., *Physics of Graphite*, Applied Science, London, 1981.
[30] Vincent, P., '*Synthèse, caractérisation, et études des propriétés d'émission de champ de nanotubes de carbone*', thesis (in french), Université Claude Bernard Lyon 1, 2002.
[31] Wang, M.S. Wang, J.Y. and Peng, L.-M., 'Engineering the cap structure of individual carbon nanotubes and corresponding electron field emission characteristics', *Appl. Phys. Lett.*, **88**, 2006, 243108.
[32] Wang M.S, Qing Chen, and Peng L.-M., 'Field emission characteristics of individual carbon nanotubes with a conical tip: the validity of the F-N theory and maximum emission current' *Small*, **4**(11), 2008, 1907–1912.
[33] Jensen, K. Weldon, J. Garcia, H. and Zettl, A. 'Nanotube Radio', *Nano Letters*, **7**(11), 2007, 3508-3511.
[34] Swanson, L.W. and Crouser, L.C., 'Effect of polyatomic adsorbates on total energy distribution of field emitted electrons', *Surf. Sci.*, **23**, 1970, 1-29.
[35] Duke, C.B. Alferieff, M.E., 'Field Emission through Atoms Adsorbed on a Metal Surface', *J. Chem. Phys.*, **46**, 1967**,** 923-937.
[36] Purcell, S.T. Vincent, P. Journet, C. and Binh, V.T. 'Tuning of nanotube mechanical resonances by electric field pulling', *Phys. Rev. Lett.*, **89**, 2002, 276103.